Multi-Contact Balancing of Humanoid Robots in Confined Spaces: Utilizing Knee Contacts

Bernd Henze, Alexander Dietrich, Máximo A. Roa, and Christian Ott

***Abstract*— Introducing humanoid robots in areas where space is limited, for example in search-and-rescue scenarios or industrial manufacturing, represents a huge challenge, especially when the environment is cluttered and unknown. The robot should be capable of utilizing multiple contact points distributed across the entire body and not just its feet and hands. Extra contacts on the whole body, for instance including the knees and elbows, enable the robot to increase its agility and robustness by enhancing the support polygon. This paper applies our passivity-based approach for hierarchical whole-body control including balancing to scenarios involving contacts distributed all over the body of the robot as required in confined spaces. The approach is experimentally validated on the torque-controlled humanoid robot TORO to demonstrate the general applicability of the presented framework.**

I. INTRODUCTION

Humanoid robots are qualified for a large variety of applications involving tasks that are often monotonic, or too dangerous for a human. Typical examples are disaster scenarios, the exploration of unknown environments, service robotics, mining, or industrial manufacturing. In order to master these situations, the robot is required to move in a highly agile and robust way, to climb stairs or industrial ladders, move through confined spaces, or traverse terrain cluttered with obstacles or debris. For achieving this, a humanoid robot should be able to balance compliantly and safely, even in the presence of unknown external disturbances. Furthermore, in order to gain a higher robustness the robot should not only use the feet to support itself, but also other parts of its body such as hands, knees, and elbows, which leads to the field of multi-contact balancing.

Common frameworks to deal with balancing on multiple contacts using all DoF (Degrees of Freedom) of the robot emerged from the field of whole-body control, either using inverse kinematics or inverse dynamics. A prioritized multitasking controller for whole-body control was presented in [1] by exploiting the concept of virtual linkage to describe the internal forces and resultant wrench on the CoM (Center of Mass). Information on the contact forces is not necessarily required, as demonstrated in [2], where an orthogonal decomposition is used to solve the inverse dynamics problem. The same approach was later reused to minimize the constraint forces in [3]. An optimization process can also be used to control the CoP (Center of Pressure) in each foot [4]. By prescribing a desired CoM trajectory and some task wrenches, the joint torques can be computed through a dynamic balance force controller [5]. A balancing controller that utilizes a hierarchical solution for solving the inverse dynamics was proposed and demonstrated in real experiments in [6]. A preview controller is presented in [7] for generating CoM trajectories, which are tracked by a task-based controller.

The authors are with the German Aerospace Center (DLR), Institute of Robotics and Mechatronics, 82234 Wessling, Germany. <firstname>.<lastname>@dlr.de

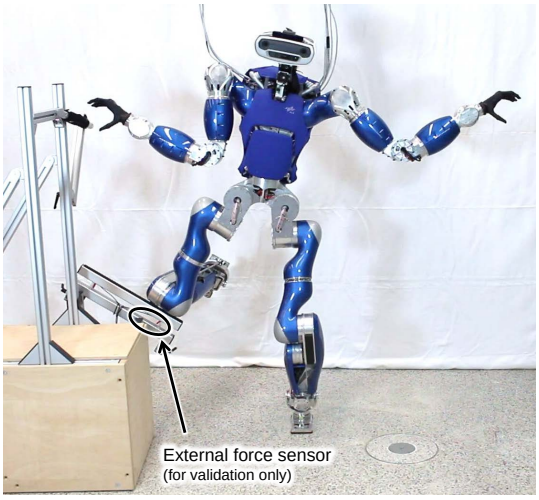

Fig. 1. Example of multi-contact balancing in confined spaces. The additional force sensor is mounted on the support structure and is only used for validation purposes.

Passivity-based approaches, which do not require the solution of inverse dynamics to deal with the balancing problem, are also known in literature. The initial approach for compliant balancing of humanoids was proposed in [8]. The idea of computing suitable ground reaction forces that are mapped to joint torques was further exploited in [9], adding orientation control to the balancing problem by exploiting structural similarities between the problems of grasping and balancing. This work was later extended by adding feedforward control in [10], which leads to a closed-loop system with a structure similar to the classical PD+ control [11]. The passivity-based framework was recently combined with hierarchical whole-body control [12], [13], enabling the robot to deal with multiple contacts as well as multiple control objectives [14]. Thus, the control framework provides the tools for the prioritization and solution of a stack of tasks concerning the serial kinematics of a humanoid robot by using null space projection methods. Balancing on multiple contacts forms a parallel mechanism within the structure of the robot, causing a redundancy in the space of contact wrenches. The resulting wrench distribution problem

is solved in [14] via a constrained quadratic optimization problem.

Introducing humanoid robots for working in confined spaces implies new challenges since the available space usually limits the motion capabilities of the rather bulky limbs of a humanoid robot. Thus, the robot should use not only hands and feet for producing deliberate contacts with the environment, but should exploit the whole body surface to gain a higher degree of robustness in the balancing and locomotion process. Adding contact points at the knees (Fig. 1), the hip, or the elbows allows the robot to enhance its support polygon and thereby achieve a more robust stance to perform an intended task, see Fig. 3. The challenge of balancing in confined spaces arises from the additional contacts, which highly constrain the motion of the robot to a submanifold in the null space of the contact constraint.

Relatively little work has been presented to explicitly consider contacts located all over the body of the robot. For example, the frameworks [1], [2], [3] control the constrained motion of the robot by accounting for the physical contact constraints, but the works do not explicitly consider contacts located all over the body of the robot. A framework based on inverse dynamics combined with an orthogonal projection was presented in [15]. The approach presented in [16] is derived from a quasi-static analysis and tested on a humanoid robot with elastic joints. Although the latter two approaches are designed to theoretically handle contacts scattered all over the body of the robot, this particular aspect has not been validated in the demonstrated experiments.

In this paper, we demonstrate that our passivity-based approach for hierarchical whole-body control [14] can also be used to operate legged humanoid robots in confined spaces. The approach regards the physical contact constraint as the task with the highest priority, as in [1], [6]. The task with the next lower priority is projected onto the null space of the Jacobian matrix representing the constraint. The third task is then projected onto the null space of the second one, and so on. One particular feature of the presented approach is that it is able to generate the required contact wrenches despite the problem of highly constrained dynamics *without the need for force-torque sensors at the contacts*. Only the external wrenches caused by a manipulation task must be measurable/observable via the internal sensors/joints of the robot. The approach is experimentally validated in different multi-contact scenarios, also included in the accompanying video. To the best of our knowledge, such skills have not been demonstrated on a real robot until now.

The remainder of this paper is structured as follows: after introducing the dynamics model in Sec. II, our passivity-based approach for hierarchical whole-body control [14] is reviewed in Sec. III-A. The consequences of using this framework in confined spaces are discussed in Sec. III-B, followed by the experimental validation on the torque-controlled humanoid robot TORO in Sec. IV. Sec. V concludes the paper.

II. DYNAMIC MODEL

The controller which will be presented below, in Sec. III, handles an arbitrary number of contacts with the environment that can be distributed all over the body of the robot. In order to deal with a contact transition or relocation, a model with floating base is used, which provides higher flexibility than a fixed-base model. In general, either the hip or the trunk represent the base link, since both parts are central bodies of the structure of the robot. The CoM can also be used as base link for legged robots [8], as the location of the CoM is crucial for balancing. Here, this concept is reused by defining a frame $\mathcal{C}$ at the CoM with the same orientation as the hip of the robot, as in [14]. Both the location and the orientation of the frame are given with respect to the world frame by the position vector $\boldsymbol{x}_\mathrm{c} \in \mathbb{R}^3$ and the rotation matrix $\boldsymbol{R}_\mathrm{c} \in \mathcal{SO}(3)$. The corresponding translational and rotational velocities are $\dot{\boldsymbol{x}}_\mathrm{c}$ and $\boldsymbol{\omega}_\mathrm{c}$, respectively. Based on the n joint angles $\boldsymbol{q} \in \mathbb{R}^n$ and $\boldsymbol{v} = (\dot{\boldsymbol{x}}_\mathrm{c}^T, \boldsymbol{\omega}_\mathrm{c}^T)^T$, the dynamics of the humanoid robot is given by

$$\boldsymbol{M} \underbrace{\begin{pmatrix} \dot{\boldsymbol{v}} \\ \ddot{\boldsymbol{q}} \end{pmatrix}}_{\dot{\boldsymbol{\nu}}} + \boldsymbol{C} \underbrace{\begin{pmatrix} \boldsymbol{v} \\ \dot{\boldsymbol{q}} \end{pmatrix}}_{\boldsymbol{\nu}} + \underbrace{\begin{pmatrix} m\boldsymbol{g}_0 \\ \boldsymbol{0} \end{pmatrix}}_{\boldsymbol{g}} = \begin{pmatrix} \boldsymbol{0} \\ \boldsymbol{\tau} \end{pmatrix} + \boldsymbol{\tau}_\mathrm{ext}. \qquad (1)$$

Herein, $\boldsymbol{M} \in \mathbb{R}^{(6+n)\times(6+n)}$ and $\boldsymbol{C} \in \mathbb{R}^{(6+n)\times(6+n)}$ are the inertia and Coriolis/centrifugal matrix, respectively. Gravity is taken into account by $\boldsymbol{g} \in \mathbb{R}^{6+n}$, containing the gravitational acceleration $\boldsymbol{g}_0 \in \mathbb{R}^6$ and the total mass m of the robot[1]. The joint torques are given by $\boldsymbol{\tau} \in \mathbb{R}^n$. The influence of external forces and torques is represented by the generalized force vector $\boldsymbol{\tau}_\mathrm{ext} \in \mathbb{R}^{6+n}$.

III. THEORY

A. Recapitulation of the Passivity-Based Approach for Hierarchical Whole-Body Control Including Balancing [14]

This section gives a brief summary of the framework presented in [14], which combines balancing with hierarchical whole-body control for legged humanoid robots.

The hierarchy in multi-objective control is defined by a stack of tasks. Each one of the tasks is described by a Jacobian matrix $\boldsymbol{J}_i \in \mathbb{R}^{m_i\times(n+6)}$ mapping the velocities in configuration space $\boldsymbol{\nu}$ to the task velocities $\dot{\boldsymbol{x}}_i \in \mathbb{R}^{m_i}$:

$$\dot{\boldsymbol{x}}_i = \boldsymbol{J}_i \boldsymbol{\nu} \qquad \forall i = 1 \dots r. \qquad (2)$$

The task with the highest priority is denoted by the index $i = 1$, and the task with the lowest one by $i = r$. In [14] we set up two different hierarchies that only differ in the order of task number two and three (see Table I). The task with the highest priority is described by the Cartesian velocities of the end effectors that are actively used for balancing by generating the wrenches $\boldsymbol{F}_\mathrm{bal}^\mathrm{cmd} \in \mathbb{R}^{m_\mathrm{bal}}$ required for supporting the weight of the robot. Note that $\boldsymbol{F}_\mathrm{bal}^\mathrm{cmd}$ stacks all forces $\boldsymbol{f}_k$ and torques $\boldsymbol{\tau}_k$ that are transmitted via the k contacts. Herein, one single contact can have up to 6 DoF.

[1]Note that $\boldsymbol{g}_0$ is six-dimensional and also contains the rotational DoFs. The structure of $\boldsymbol{g}$ is caused by the choice of $\mathcal{C}$ as base frame (see [8]).

The next two tasks consist of two Cartesian compliances $\boldsymbol{F}_{\text{c}}^{\text{cpl}} \in \mathbb{R}^{m_{\text{c}}}$ and $\boldsymbol{F}_{\text{int}}^{\text{cpl}} \in \mathbb{R}^{m_{\text{int}}}$, which stabilize the CoM frame $\mathcal{C}$ and the remaining end effectors, that can be used to perform an interaction task. The exact definition of both compliances can be found in [10]. The last task ($i = 4$) is given by a joint-space compliance $\boldsymbol{\tau}_{\text{pose}}^{\text{cpl}} \in \mathbb{R}^n$ that stabilizes the posture of the robot to avoid drifting.

TABLE I
APPLIED TASK HIERARCHY COMPARED WITH [14].

Level i	"Int. over CoM" [14]	"CoM over Int." [14]	Confined Spaces
1	$\boldsymbol{J}_{\text{bal}}$, $\boldsymbol{F}_{\text{bal}}^{\text{cmd}}$	$\boldsymbol{J}_{\text{bal}}$, $\boldsymbol{F}_{\text{bal}}^{\text{cmd}}$	$\boldsymbol{J}_{\text{bal}}$, $\boldsymbol{F}_{\text{bal}}^{\text{cmd}}$
2	$\boldsymbol{J}_{\text{int}}$, $\boldsymbol{F}_{\text{int}}^{\text{cpl}}$	$\boldsymbol{J}_{\text{c}}$, $\boldsymbol{F}_{\text{c}}^{\text{cpl}}$	$\boldsymbol{J}_{\text{c}}$, $\boldsymbol{J}_{\text{int}}$, $\boldsymbol{F}_{\text{c}}^{\text{cpl}}$, $\boldsymbol{F}_{\text{int}}^{\text{cpl}}$
3	$\boldsymbol{J}_{\text{c}}$, $\boldsymbol{F}_{\text{c}}^{\text{cpl}}$	$\boldsymbol{J}_{\text{int}}$, $\boldsymbol{F}_{\text{int}}^{\text{cpl}}$	$\boldsymbol{J}_{\text{pose}}$, $\boldsymbol{\tau}_{\text{pose}}^{\text{cpl}}$
4	$\boldsymbol{J}_{\text{pose}}$, $\boldsymbol{\tau}_{\text{pose}}^{\text{cpl}}$	$\boldsymbol{J}_{\text{pose}}$, $\boldsymbol{\tau}_{\text{pose}}^{\text{cpl}}$	-

Based on the task definition, the so-called augmented Jacobian matrix can be computed

$$\boldsymbol{J}_j^{\text{aug}} = \begin{bmatrix} \boldsymbol{J}_1 \\ \vdots \\ \boldsymbol{J}_j \end{bmatrix}, \tag{3}$$

which stacks all Jacobian matrices of the tasks with equal or higher priority ($i = 1 \dots j$). The augmented Jacobian matrix can then be used to compute the null space base matrix $\boldsymbol{Z}_i$, with $\boldsymbol{J}_{i-1}^{\text{aug}} \boldsymbol{Z}_i^T$ as detailed in [13], [17]. Again, $\boldsymbol{Z}_i$ can be used to compute a null space projector $\boldsymbol{N}_i \in \mathbb{R}^{(6+n)\times(6+n)}$ that maps the control actions on level i onto the null space of all task Jacobian matrices with a higher priority ($1 \dots (i-1)$). Applying these steps, for example, to the particular task hierarchy "Int. over CoM" given in Table I leads to

$$\begin{pmatrix} m\boldsymbol{g}_0 \\ -\boldsymbol{\tau} \end{pmatrix} = \underbrace{\begin{bmatrix} \boldsymbol{J}_{\text{bal}}^T & \boldsymbol{N}_2\boldsymbol{J}_{\text{int}}^T & \boldsymbol{N}_3\boldsymbol{J}_c^T & \boldsymbol{N}_4\boldsymbol{J}_{\text{pose}}^T \end{bmatrix}}_{\boldsymbol{\Xi} = \begin{bmatrix} \boldsymbol{\Xi}_u \\ \boldsymbol{\Xi}_l \end{bmatrix}} \underbrace{\begin{pmatrix} \boldsymbol{F}_{\text{bal}}^{\text{cmd}} \\ \boldsymbol{F}_{\text{int}}^{\text{cpl}} \\ \boldsymbol{F}_{\text{c}}^{\text{cpl}} \\ \boldsymbol{\tau}_{\text{pose}}^{\text{cpl}} \end{pmatrix}}_{\boldsymbol{F}}. \tag{4}$$

Herein, the mapping $\boldsymbol{\Xi} \in \mathbb{R}^{(6+n)\times\sigma}$ is partitioned into $\boldsymbol{\Xi}_u \in \mathbb{R}^{6\times\sigma}$ and $\boldsymbol{\Xi}_l \in \mathbb{R}^{n\times\sigma}$.

In order to account for the under-actuation of the base, $\boldsymbol{F}_{\text{bal}}^{\text{cmd}}$ must be chosen such that $m\boldsymbol{g}_0 = \boldsymbol{\Xi}_u \boldsymbol{F}$ holds by minimizing the quadratic cost function

$$\min_{\boldsymbol{F}_{\text{bal}}^{\text{cmd}}} \left(\boldsymbol{F}_{\text{bal}}^{\text{cmd}} - \boldsymbol{F}_{\text{bal}}^{\text{def}}\right)^T \boldsymbol{Q} \left(\boldsymbol{F}_{\text{bal}}^{\text{cmd}} - \boldsymbol{F}_{\text{bal}}^{\text{def}}\right) \tag{5}$$

with respect to $m\boldsymbol{g}_0 = \boldsymbol{\Xi}_u \boldsymbol{F}$, to the contact model

$$\begin{aligned} f_{k,z}^{\min} \le f_{k,z} \le f_{k,z}^{\max}, \\ \boldsymbol{p}_k \in \mathcal{S}_k, \\ \left|f_{k,x/y}\right| \le \tilde{\mu}_k f_{k,z} \end{aligned} \tag{6}$$

for all k balancing contacts, and to the constraint

$$\left|\boldsymbol{\Xi}_l \boldsymbol{F}\right| \le \boldsymbol{\tau}^{\max}. \tag{7}$$

The variables in (6) are given with respect to a local, body-fixed coordinate system of the k-th contact, whose z-axis is perpendicular to the surface of the contact. The first equation in (6) accounts for the unilaterality of the contact by restricting the perpendicular contact force $f_{k,z}$ to be larger than a minimum value $f_{k,z}^{\min}$. The second line confines the CoP $\boldsymbol{p}_k$ in each contact to the corresponding contact area $\mathcal{S}_k$. The third line avoids any slipping of the contact by limiting the amplitude of the tangential forces $f_{k,x}$ and $f_{k,y}$ to a friction pyramid characterized by $\tilde{\mu}_k$ (see [14]). The control torque is limited by $\boldsymbol{\tau}^{\max}$ via (7). After obtaining $\boldsymbol{F}_{\text{bal}}^{\text{cmd}}$ from (5), the control torque $\boldsymbol{\tau}$ is computed via $\boldsymbol{\tau} = -\boldsymbol{\Xi}_l \boldsymbol{F}$ as suggested by (4).

Inserting (4) into (1) leads to a decoupled closed-loop dynamics

$$\boldsymbol{\Lambda}\dot{\boldsymbol{v}} + \boldsymbol{\mu}\boldsymbol{v} + \begin{pmatrix} \boldsymbol{F}_1 \\ \boldsymbol{Z}_2\boldsymbol{J}_2^T\boldsymbol{F}_2 \\ \vdots \\ \boldsymbol{Z}_r\boldsymbol{J}_r^T\boldsymbol{F}_r \end{pmatrix} = \bar{\boldsymbol{J}}^{-T}\boldsymbol{\tau}_{\text{ext}} \tag{8}$$

based on local, hierarchy-consistent null space velocities $\boldsymbol{v}_1$ to $\boldsymbol{v}_r$ given by

$$\underbrace{\begin{pmatrix} \boldsymbol{v}_1 \\ \vdots \\ \boldsymbol{v}_r \end{pmatrix}}_{\boldsymbol{v}} = \underbrace{\begin{bmatrix} \bar{\boldsymbol{J}}_1 \\ \vdots \\ \bar{\boldsymbol{J}}_r \end{bmatrix}}_{\bar{\boldsymbol{J}}} \boldsymbol{\nu}. \tag{9}$$

The computation of $\bar{\boldsymbol{J}}$ and $\bar{\boldsymbol{J}}^{-1} = \left[\boldsymbol{J}_1^{M+}, \boldsymbol{Z}_2^T, \dots, \boldsymbol{Z}_r^T\right]$ with $\boldsymbol{J}_1^{M+}$ denoting the dynamically consistent pseudo-inverse is detailed in [13], [17], [14].

B. Hierarchical Whole-Body Control in the Context of Confined Spaces

In our previous work [14], we assumed that the robot only uses its end effectors to generate the necessary balancing wrenches $\boldsymbol{F}_{\text{bal}}^{\text{cmd}}$. But due to the limited maneuverability in confined spaces, the robot needs to be able to exploit also contacts that might be located somewhere on the robot structure, and not only at the end effectors. Thus, in this work we will allow the contacts to be scattered all over the surface of the robot, as schematically depicted in Fig. 2a. In consequence, the motion of the CoM and the interaction points are constrained to a submanifold of Cartesian space (dashed green lines in Fig. 2a) defined by the physical constraint stating that the balancing end effectors are at rest ($\dot{\boldsymbol{x}}_{\text{bal}} = \boldsymbol{J}_{\text{bal}}\,\boldsymbol{\nu} = \boldsymbol{0}$).

In order to meet this requirement, we implement a hierarchy similar to the one used in [14], see Table I. In [14], we studied the effect of changing the order of the CoM and the interaction task, leading to the conclusion that both are beneficial depending on the scenario that the robot is facing. Here, we will arrange the CoM and the interaction end effectors together on the second level of the hierarchy. The task with the highest priority consists of the generation of suitable contact wrenches $\boldsymbol{F}_{\text{bal}}^{\text{cmd}}$ for supporting the robot.

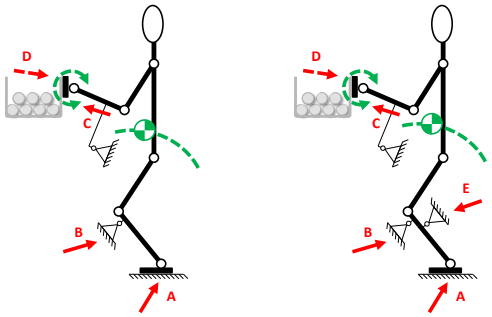

(a) (b)

Fig. 2. Examples of contact situations with external forces and torques acting all over the body of the robot (balancing contacts: A, B, C, E; interaction points: D). The green dashed lines represent the manifold to which the CoM and the interaction points are constrained by the balancing contacts. The interaction wrench in D has a component which is perpendicular to the manifold. The balancing wrenches in b) are overdetermined due to the redundant definition of the wrenches in B and E.

The joint-space compliance $\boldsymbol{\tau}_{\text{pose}}^{\text{cpl}}$ is located on the lowest priority level.

In [14] we used the hierarchical control framework to minimize the dynamic coupling between the tasks for balancing, CoM, and interaction. But those three tasks were not conflicting on a kinematic level. Only the last tasks ($\boldsymbol{\tau}_{\text{pose}}^{\text{cpl}}$) posed a kinematic conflict with the ones on top of it. In the context of confined spaces, there are additional kinematic conflicts arising. As already mentioned, the additional contact points on the surface of the robot constrain the motion of the CoM and the interaction end effectors to a submanifold of Cartesian space. Thus, there already exists a kinematical conflict between the balancing task ($i = 1$) and the CoM/interaction task ($i = 2$). The consequence is that the computation of the null space projector for $\boldsymbol{\tau}_{\text{pose}}^{\text{cpl}}$ becomes more cumbersome due to the fact that the corresponding $\boldsymbol{J}_j^{\text{aug}}$ becomes rank-deficient.

Another aspect of operating a robot in confined spaces is the influence of external forces. Assuming a static configuration $\dot{\boldsymbol{\nu}} = \boldsymbol{\nu} = \boldsymbol{0}$ and that all external wrenches act solely on the balancing contacts and interaction points, the last line of (8) simplifies to

$$\boldsymbol{F}_{\text{bal}}^{\text{cmd}} = \boldsymbol{J}_{\text{bal}}^{M+,T} \left(\boldsymbol{J}_{\text{bal}}^T \boldsymbol{F}_{\text{bal}} + \boldsymbol{J}_{\text{int}}^T \boldsymbol{F}_{\text{int}} \right). \tag{10}$$

1) Analysis of the Balancing Wrenches: Let us first consider the case where no external forces and torques act on the robot except for the balancing wrenches $\boldsymbol{F}_{\text{bal}}^{\text{cmd}}$. Under this assumption, (10) simplifies to $\boldsymbol{F}_{\text{bal}}^{\text{cmd}} = \boldsymbol{J}_{\text{bal}}^{M+,T} \boldsymbol{J}_{\text{bal}}^T \boldsymbol{F}_{\text{bal}}$. If $\boldsymbol{J}_{\text{bal}}$ is of full rank, we can conclude that for a static configuration the commanded balancing wrenches $\boldsymbol{F}_{\text{bal}}^{\text{cmd}}$ are identical to the external ones $\boldsymbol{F}_{\text{bal}}$. If $\boldsymbol{J}_{\text{bal}}$ is rank-deficient, it can happen that $\boldsymbol{F}_{\text{bal}}$ deviates from $\boldsymbol{F}_{\text{bal}}^{\text{cmd}}$. Therefore, the contacts can lift off, slip, or tilt although the commanded balancing wrenches $\boldsymbol{F}_{\text{bal}}^{\text{cmd}}$ are subjected to the contact model (6). Thus, it is possible that the robot falls over. There are basically two methods to counteract this problem: First, the contact points can be chosen such that $\boldsymbol{J}_{\text{bal}}$ is of full rank. Fig. 2b shows an example leading to a rank-deficient $\boldsymbol{J}_{\text{bal}}$ due to the redundant definition of the contact points B and E. The second method is to parameterize and/or modify the optimization (5) such that $\boldsymbol{F}_{\text{bal}}^{\text{cmd}}$ is chosen close enough to $\boldsymbol{F}_{\text{bal}}$. For example, one can choose a symmetric force distribution if the configuration of the robot is also symmetric.

TABLE II

PARAMETERS USED FOR THE OPTIMIZATION.

	$\boldsymbol{Q}$			
FootR/L	$\text{diag}(10^{-3}\, 10^{-3}\, 10^{-3}\, 1\, 1\, 1)$			
HandR/L	$\text{diag}(\frac{1}{40}\, \frac{1}{40}\, \frac{1}{40}, 1, 1, 1)$			
KneeR/L	$\text{diag}(10^{-3}\, 10^{-3}\, 10^{-3}\, 1\, 1\, 1)$			
	$f_{k,z}^{\min}, f_{k,z}^{\max}$ [N]	$\tilde{\mu}_k$	$p_{\text{k,x}}^{\min}, p_{\text{k,x}}^{\max}$ [m]	$p_{\text{k,y}}^{\min}, p_{\text{k,y}}^{\max}$ [m]
FootR/L	$50, 900$	0.4	$-0.07, 0.13$	$-0.045, 0.045$
HandR/L	$20, 100$	–	–	–
KneeR/L	$50, 900$	0.4	$-0.15, 0.03$	$-0.015, 0.015$

2) Analysis of the Interaction Wrenches: Even if $\boldsymbol{J}_{\text{bal}}$ is of full rank as discussed in Sec. III-B.1, it can happen that $\boldsymbol{F}_{\text{bal}}^{\text{cmd}}$ deviates from $\boldsymbol{F}_{\text{bal}}$ due to dynamic effects or the influence of the interaction wrenches. For a static configuration, multiplying the first line of (10) with $\boldsymbol{J}_{\text{bal}}^T$ leads to

$$\boldsymbol{J}_{\text{bal}}^T \boldsymbol{F}_{\text{bal}}^{\text{cmd}} = \boldsymbol{J}_{\text{bal}}^T \boldsymbol{F}_{\text{bal}} + \boldsymbol{J}_{\text{bal}}^T \boldsymbol{J}_{\text{bal}}^{M+,T} \boldsymbol{J}_{\text{int}}^T \boldsymbol{F}_{\text{int}} \tag{11}$$

considering $\boldsymbol{J}_{\text{bal}}^{M+,T} \boldsymbol{J}_{\text{bal}}^T = \boldsymbol{I}$. As one can see, a deviation between $\boldsymbol{F}_{\text{bal}}^{\text{cmd}}$ and $\boldsymbol{F}_{\text{bal}}$ can occur if $\boldsymbol{F}_{\text{int}}$ has a component that is perpendicular to the submanifold on which the motion of the CoM and the interaction end effectors takes place (see C and D in Fig. 2b). In simpler terms, the balancing wrenches can deviate if $\boldsymbol{F}_{\text{int}}$ is acting in a direction in which the robot cannot move. Analogously $\boldsymbol{F}_{\text{int}}^{\text{cpl}}$ will also deviate from $\boldsymbol{F}_{\text{int}}$. Of course, this problem does not only exist in confined spaces, but it becomes more and more prominent with a higher number of contact constraints imposed on the robot, as it is the nature of confined spaces. Alternatives for dealing with this problem can be the explicit measurement of interaction wrenches by additional sensors as e.g. FTSs or a sensitive skin.

IV. EXPERIMENTS

To verify the performance of our control framework in confined spaces, four experiments were performed on the humanoid robot TORO, which has a height of $1.74\,\text{m}$ and a weight of $76.4\,\text{kg}$ [18], [19]. It has 27 DoF (not counting the hands); the 25 joints located in the legs, arms and hip are based on the technology of the DLR-KUKA LBR (Lightweight robot arm), and can be operated in both position and torque control mode [20]. The two additional DoF, located in the neck of the robot, are implemented with servo motors. The robot is equipped with position and torque sensors in the joints based on the LBR drives, and also has force-torque sensors at the feet and an IMU to measure the orientation and angular velocity of the hip. The algorithm for estimating the state of the base frame is detailed in [10].

The experiments use the feet, hands, and knees to support the weight of the robot. The 25 LBR joints are operated

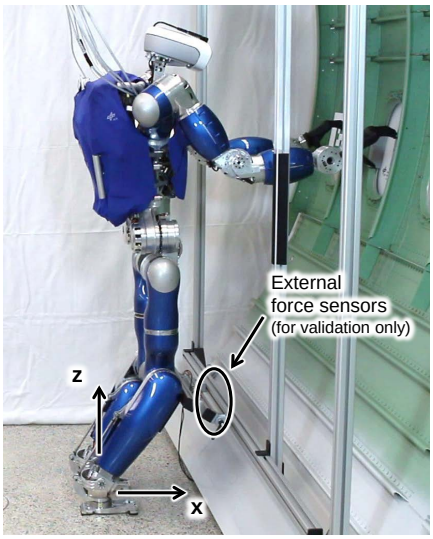

Fig. 3. Setup of Experiment I. The support polygon is extended by the additional contacts at the knees. Additional force sensors are mounted on the aircraft fuselage only for validation purposes.

in torque-controlled mode. The two joints in the neck are not relevant for the experiments. The proposed controller is implemented in MATLAB/Simulink, using qpOASES [21] to solve the constraint quadratic optimization problem. The controller is executed at a rate of 1 kHz. The parameters used by the optimization are listed in Table II. The compliances are parametrized as in [10].

In Experiment I, II, and III, the robot uses the all 6 Cartesian DoF of the feet for balancing. For the contacts at the knees and the hands, the robot is only allowed to generate forces perpendicular to the contact surface ($f_{k,z}$) in order to account for environments with low friction. In Experiment IV, the robot balances solely on the knees by exploiting all 6 DoF of the knee contacts. Note that all contacts are described by a contact model, as specified by (6) and Table II. The interaction task in all three experiments demands that the corresponding hands and feet maintain their position and orientation relative to the world. In order to achieve smooth contact transition, a state machine was implemented to ramp $\boldsymbol{Q}$ and $\boldsymbol{F}_{\text{bal}}^{\text{def}}$ in (5), modify $\boldsymbol{\Xi}$, and (de-)activate the contact model (6) in a coordinated sequence.

A video of the experiments can be found in the multimedia attachment of this manuscript.

A. Experiment I: Extending the Support Polygon

The first experiment shows an application from the field of industrial manufacturing, in which the robot has to perform an assembly task within the fuselage of an airplane[2]. As shown in Fig. 3, the robot stands in front of the fuselage section and has to reach for the hull with the hands. However, the robot is only able to shift the CoM to the front of the support polygon given by the convex hull of the feet, which limits the reach of its arms. In order to overcome this impediment, the robot lowers its CoM until the knees establish contact with the hull. Note that in this experiment the optimization is only allowed to generate forces perpendicular to the contact surface at the knees ($f_{\text{KneeR/L,z}}$). With the additional contact at its knees, the robot can now shift its CoM even in front of the support polygon spanned by the feet, which significantly increases the range of the arms.

[2]See COMANOID project: `http://comanoid.cnrs.fr` (H2020-ICT-645097 COMANOID)

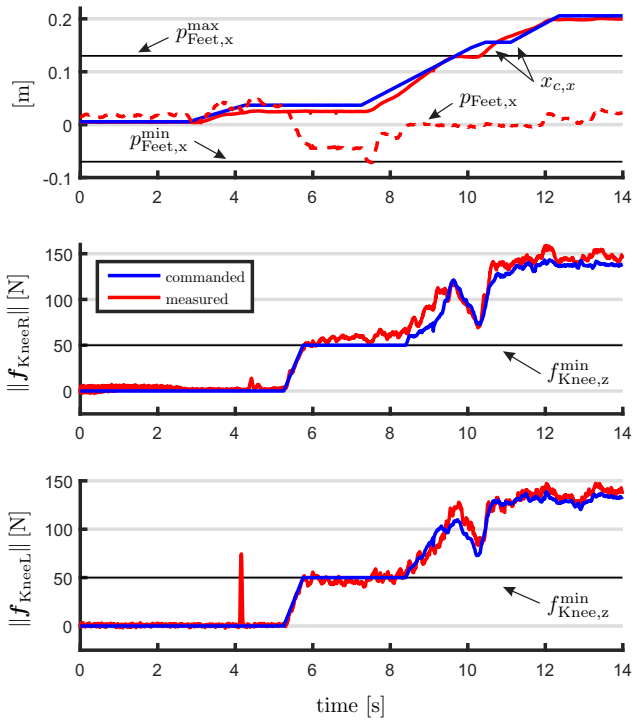

Fig. 4. Position of the CoM, the CoP of the feet, and the knee forces during Experiment I.

The telemetry data recorded during the experiment are shown in Fig. 4. The additional knee contacts are enabled at $t = 5\,\text{s}$, which caused the forces at the knees to rise from 0 N (deactivated state) up to 138 N (right) and 136 N (left). In order to validate the contact forces, the experimental setup was equipped with two additional external force sensors measuring the contact forces at the knees (see Fig. 4). Note that those sensors are only used for verification and not for the control loop; the contact forces computed by the optimization ($f^{\text{cmd}}_{\text{KneeR/L,z}}$) match quite well with the forces measured by the sensors ($f_{\text{KneeR/L,z}}$), as shown in Fig. 4. The slight difference of 16 N and 13 N is mainly due to modelling errors and imprecise sensor calibration. Note that the spike at $t = 4\,\text{s}$ in the measured force for the left knee is caused by the impact when the robot hits the bar by lowering the CoM. Note also that the position of the CoP of the feet changes during the motion. First, the CoP moves 4.5 cm to the front simultaneously with the CoM. After the knee contacts are enabled ($t = 5\,\text{s}$), the CoP moves to the back in order to provide the minimum contact force for the knees. As soon as the knee forces are rising, the CoP moves to zero. The reason for this is that the controller is configured to generate mainly forces instead of torques (see Table II).

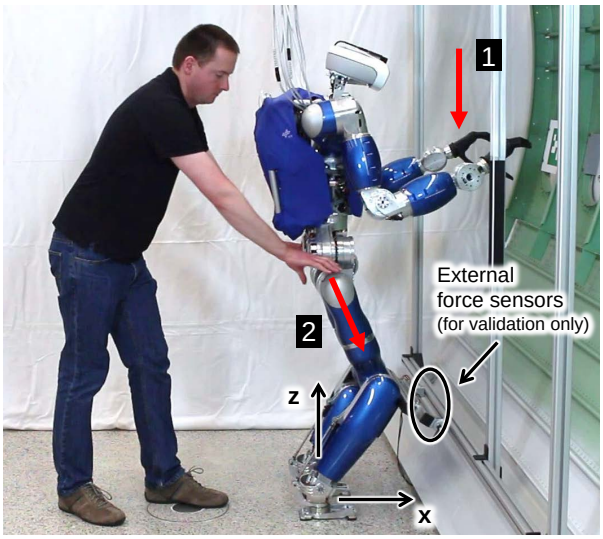

Fig. 5. Setup of Experiment II. The red arrows represent the applied external forces.

Despite supporting the weight of the robot, the additional knee forces generate a torque about the ankle axes such that the controller no longer needs to produce a torque at the sole of the feet. Apart from an increased robustness of the stance, the contacts at the knees allow the robot to shift its CoM up to $x_{c,x} = 20.5\,\mathrm{cm}$, which is $7.5\,\mathrm{cm}$ in front of the support polygon of the feet characterized by $p^{\min}_{\mathrm{FootR/L,x}}$ and $p^{\max}_{\mathrm{FootR/L,x}}$. The difference between the desired and the measured CoM location during the motion is caused by the fact that the desired position is commanded on a straight line in the sagittal plane, while the real CoM can only move along the submanifold determined by the contact constraints (as explained later in detail in Experiment IV). In summary, the knees increase the operating range of both the CoM and the arms, which allows the robot to fulfill its designated manufacturing task.

B. Experiment II: Influence of External Forces

In this experiment the robot is again positioned in front of the aircraft fuselage as in the first experiment (see Fig. 5), but this time, external disturbances are manually applied to the robot. In the first half of the experiment ($t < 11\,\mathrm{s}$), an external force is applied twice to the hands (1^{st}: $71\,\mathrm{N}$, 2^{nd}: $78\,\mathrm{N}$). The wrenches caused by the compliance $\boldsymbol{F}^{\mathrm{cpl}}_{\mathrm{int}}$ are immediately counteracted by the balancing wrenches $\boldsymbol{F}^{\mathrm{cmd}}_{\mathrm{bal}}$, as shown in Fig. 6. Note that the commanded and measured forces have a very good match despite minor discrepancies, mainly due to modelling errors and imprecise sensor calibration. As explained in Sec. III-B.2, the additional contacts at the knees constrain the motion of the hip but not of the hands. Thus, the balancing forces $\boldsymbol{F}_{\mathrm{bal}}$ match the commanded ones $\boldsymbol{F}^{\mathrm{cmd}}_{\mathrm{bal}}$.

In the second half of the experiment ($t > 11\,\mathrm{s}$), the external forces are applied at the hip, in a direction parallel to the thigh. As the robot cannot move in this particular direction due to the knee contacts, there is a deviation

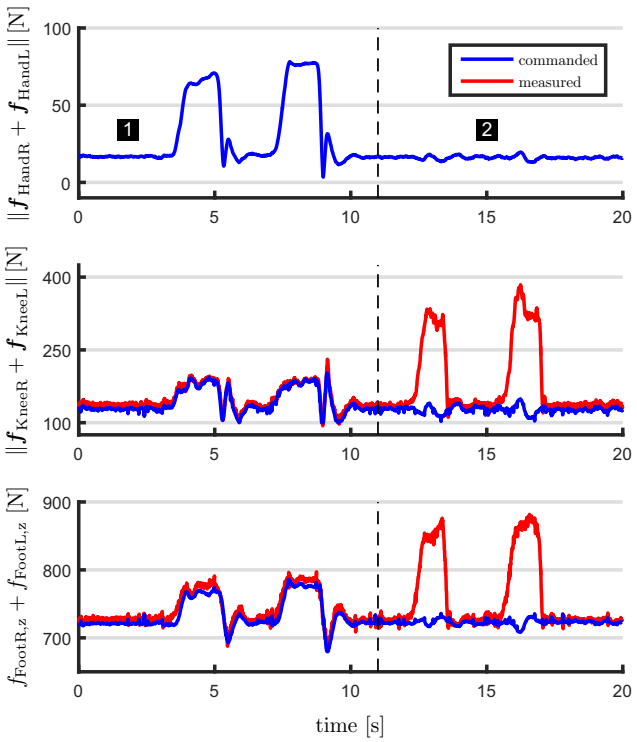

Fig. 6. Contact forces at the hands, the knees, and the feet during Experiment II.

between $\boldsymbol{F}_{\mathrm{bal}}$ and $\boldsymbol{F}^{\mathrm{cmd}}_{\mathrm{bal}}$. The influence of the external force on $\boldsymbol{F}^{\mathrm{cmd}}_{\mathrm{bal}}$ is minimal, as shown in Fig. 5. However, the real contact wrenches $\boldsymbol{F}_{\mathrm{bal}}$ rise up to $384\,\mathrm{N}$ for the knees and $882\,\mathrm{N}$ for the feet. This indicates that the problem of non-measurable/observable external forces increases in the case of confined spaces, as discussed in Sec. III-B.2.

C. Experiment III: Replacing one Foot with a Knee

The second experiment presents the robot in a highly asymmetric pose (see Fig. 1 and Fig. 7): The robot starts with both feet on the ground (phase 1) and brings the right hand into contact with a support structure (phase 2), which is required for lifting the right foot in phase 3. In phase 4, the knee is bent back and placed on an additional external force sensor mounted on the support structure. Again, the sensor is only used for verification and not for control. In phase 5, the hand contact is removed, such that the robot balances only on the left foot and the right knee. Note that in this experiment the optimization is only allowed to generate forces perpendicular to the contact surface at the knee ($f_{\mathrm{KneeR,z}}$).

Fig. 8 shows the recorded data: the hand contact is activated at $t = 7\,\mathrm{s}$, which causes $f_{\mathrm{HandR,z}}$ to rise to its minimum specified value $f^{\min}_{\mathrm{Hand,z}}$. When the right foot is lifted (phase 2), the load on the left leg increases from $474\,\mathrm{N}$ to $810\,\mathrm{N}$. The force in the right hand increases to values between $25\,\mathrm{N}$ and $50\,\mathrm{N}$ in order to counteract the torque, which is induced by the horizontal distance between CoM and the left foot. As soon as the right knee hits the support structure, there is an impact in the measured contact

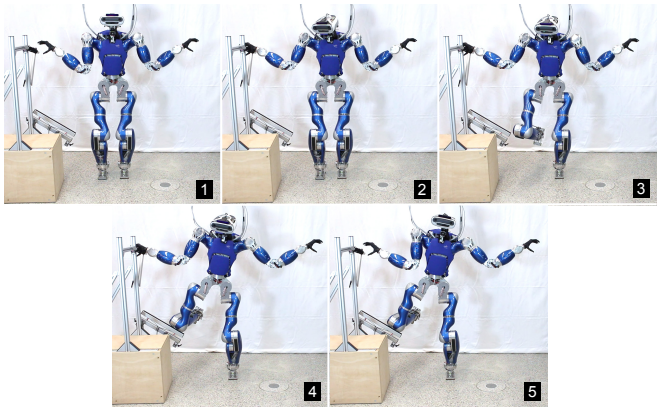

Fig. 7. Motion sequence during Experiment III. The robot lifts its right foot and places its right knee on the support structure.

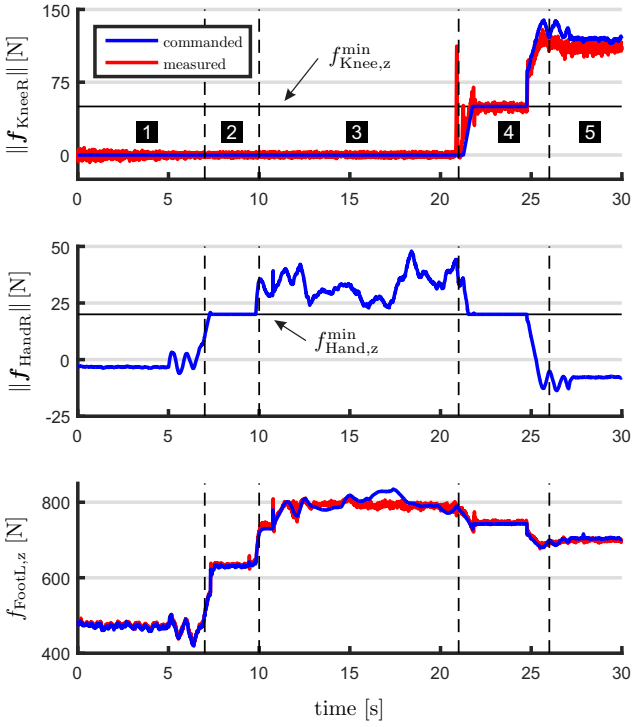

Fig. 8. Contact forces at the hands, the knees, and the feet during Experiment III.

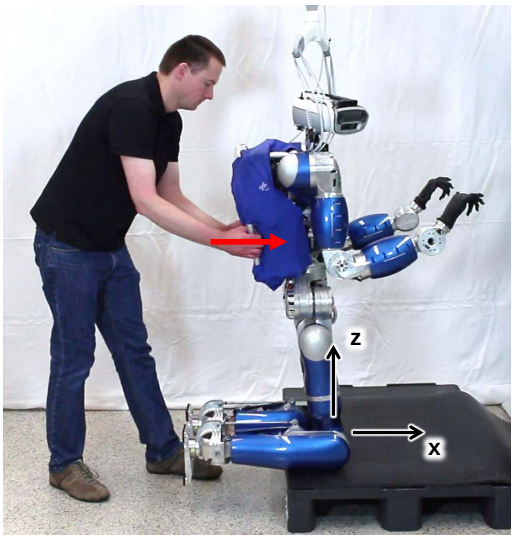

Fig. 9. Setup of Experiment IV. The robot balances solely on the knees. The red arrow represents the applied disturbance.

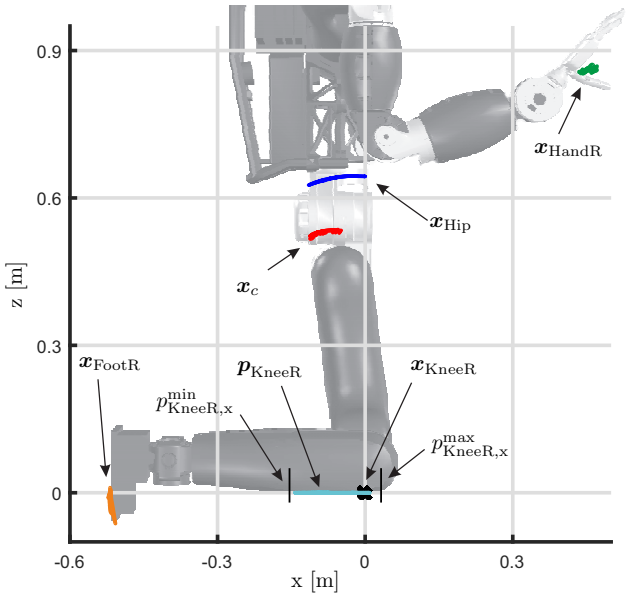

Fig. 10. Trajectory of several prominent points in the sagittal plane of the robot during Experiment IV.

forces at $t = 20\,\text{s}$. Activating the right knee for balancing reduces the force in the right hand again to its minimum of $f^{\min}_{\text{HandR,z}} = 20\,\text{N}$. The reason for this is that the cost function is parameterized such that the use of the hands is rather costly (see Table II). Thus, the controller redistributes the load of the right hand to the right knee as much as possible (120 N). Of course, this also lowers the load of the left foot to 705 N, as the right knee contributes to carrying the weight of the robot. Again, the commanded and measured contact forces at the knees and at the feet match quite well, apart from minor discrepancies as in the previous experiments. The experiment shows that using the right knee for balancing is more efficient than using the right hand because the knee can also carry a share of the weight of the robot, while the right hand can only contribute to control the CoM horizontally.

D. Experiment IV: Balancing Solely on Knees

This experiment validates the capability of TORO to balance solely on its knees, as shown in Fig. 9. In order to allow the robot to generate a sufficient set of balancing wrenches, the optimization is configured such that it can distribute the load to all 6 DoF at each knee. But due to $\boldsymbol{N}_2$, $\boldsymbol{N}_3$, and $\boldsymbol{N}_4$, the compliances influence the contact wrenches only in the directions that can actually be generated. Note that TORO has a flat area of $0.18\,\text{cm}$ by $0.3\,\text{cm}$ at the top of its shin, which is used as contact surface $\mathcal{S}_{\text{KneeR/L}}$ during the

experiment. Starting from the initial configuration, the robot is disturbed by manually moving the backpack, as shown in Fig. 9. The results are given in Fig. 10 in terms of the location of the CoM, hip, right hand, right knee, and right foot in the sagittal plane of the robot. Note that the right knee does not move due to the constraint $\boldsymbol{v}_{\text{bal}} = \mathbf{0}$. The right hand and the right foot are kept stationary with respect to the world by the controller. Because of the constrained kinematics, the hip can only be moved on a circular curve as shown in Fig. 10. The same holds for the CoM, which is roughly $11\,\text{cm}$ below the hip. The manually induced motion exploits almost the complete range of admissible CoP locations available at the knee contacts ($p^{\text{min}}_{\text{KneeR,x}} \leq p_{\text{KneeR,x}} \leq p^{\text{max}}_{\text{KneeR,x}}$).

V. CONCLUSION

This work demonstrates the application of our passivity-based approach for hierarchical whole-body control to operating legged humanoid robots in confined spaces, i.e. areas in which the robot has very limited space to maneuver. Thus, the robot is forced to use not only the hands and feet for balancing, but also contacts that are located all over the body of the robot such as knees, elbows and shoulders. The ability to handle contacts distributed all over the body of the robot potentially opens new modes of locomotion, such as crawling or wedging the robot into cramped spaces.

The applied hierarchy sorts a set of tasks with different priorities. The task with the highest priority is the generation of suitable contact wrenches required for supporting and moving the robot. Due to the high number of contacts, the motion of the robot is constrained to a submanifold determined by the physical contact constraint. This implies that the task on the second priority level must operate in the null space of the Jacobian matrix given by the contact constraint. The task with the third priority level is then projected onto the null space of the second, and so on. This implies that tasks with a lower priority level lower then the contact constraint share the null space of the constraint according to their relative priority level. One advantage of the framework is that it can generate sufficient contact wrenches to keep the balance, even in highly constrained contact situations. It can also handle external disturbances as long as their effect is not perpendicular to the submanifold given by the contact constraint. The approach has been validated in various experiments on multi-contact balancing, as illustrated in the accompanying video.

The problem of a robot moving in highly constrained multi-contact situations has some similarities to a robot in a singular configuration, as in both cases the robot suffers from limited freedom of movement. Further investigation of these similarities is the next step along this line of research.

ACKNOWLEDGMENT

This work was partially supported by the European Commission (H2020-ICT-645097 COMANOID).

The authors would like to thank Robert Burger and Florian Schmidt for the support on the real-time software aspects related to the humanoid robot TORO.

REFERENCES

[1] L. Sentis, J. Park, and O. Khatib, "Compliant control of multicontact and center-of-mass behaviors in humanoid robots," *IEEE Trans. on Robotics*, vol. 26, no. 3, pp. 483–501, 2010.

[2] M. Mistry, J. Buchli, and S. Schaal, "Inverse dynamics control of floating base systems using orthogonal decomposition," in *IEEE Int. Conf. on Robotics and Automation*, 2010, pp. 3406–3412.

[3] L. Righetti, J. Buchli, M. Mistry, M. Kalakrishnan, and S. Schaal, "Optimal distribution of contact forces with inverse-dynamics control," *Int. J. of Robotics Research*, vol. 32, no. 3, pp. 280 – 298, 2013.

[4] P. M. Wensing, G. B. Hammam, B. Dariush, and D. E. Orin, "Optimizing foot centers of pressure through force distribution in a humanoid robot," *Int. J. of Humanoid Robotics*, vol. 10, no. 03, 2013.

[5] B. J. Stephens and C. G. Atkeson, "Dynamic balance force control for compliant humanoid robots," in *IEEE/RSJ Int. Conf. on Intelligent Robots and Systems*, 2010, pp. 1248–1255.

[6] A. Herzog, N. Rotella, S. Mason, F. Grimminger, S. Schaal, and L. Righetti, "Momentum control with hierarchical inverse dynamics on a torque-controlled humanoid," *Autonomous Robots*, pp. 1 – 19, 2015.

[7] H. Audren, J. Vaillant, A. Kheddar, A. Escande, K. Kaneko, and E. Yoshida, "Model preview control in multi-contact motion – application to a humanoid robot," in *IEEE/RSJ Int. Conf. on Intelligent Robots and Systems*, 2014, pp. 4030 – 4035.

[8] S.-H. Hyon, J. G. Hale, and G. Cheng, "Full-body compliant human-humanoid interaction: Balancing in the presence of unknown external forces," *IEEE Trans. on Robotics*, vol. 23, no. 5, pp. 884 – 898, 2007.

[9] C. Ott, M. A. Roa, and G. Hirzinger, "Posture and balance control for biped robots based on contact force optimization," in *IEEE-RAS Int. Conf. on Humanoid Robots*, 2011, pp. 26 – 33.

[10] B. Henze, M. A. Roa, and C. Ott, "Passivity-based whole-body balancing for torque-controlled humanoid robots in multi-contact scenarios," *Int. J. of Robotic Research*, vol. 35, no. 2, pp. 1522 – 1543, 2016.

[11] B. Paden and R. Panja, "Globally asymptotically stable 'PD+' controller for robot manipulators," *Int. J. of Control*, vol. 47, no. 6, pp. 1697 – 1712, 1988.

[12] A. Dietrich, C. Ott, and A. Albu-Schäffer, "Multi-Objective Compliance Control of Redundant Manipulators: Hierarchy, Control, and Stability," in *IEEE/RSJ Int. Conf. on Intelligent Robots and Systems*, 2013, pp. 3043–3050.

[13] C. Ott, A. Dietrich, and A. Albu-Schäffer, "Prioritized multi-task compliance control of redundant manipulators," *Automatica*, vol. 53, pp. 416 – 423, 2015.

[14] B. Henze, A. Dietrich, and C. Ott, "An approach to combine balancing with hierarchical whole-body control for legged humanoid robots," *IEEE Robotics and Automation Letters*, vol. 1, no. 2, pp. 700 – 707, 2016.

[15] F. Aghili and C.-Y. Su, "Control of constrained robots subject to unilateral contacts and friction cone constraints," in *IEEE Int. Conf. on Robotics and Automation*, 2016, pp. 2347 – 2352.

[16] E. Farnioli, M. Gabiccini, and A. Bicchi, "Toward whole-body loco-manipulation: Experimental results on multi-contact interaction with the walk-man robot," in *IEEE/RSJ Int. Conf. on Intelligent Robots and Systems*, 2016, pp. 2347 – 2352.

[17] A. Dietrich, *Whole-Body Impedance Control of Wheeled Humanoid Robots*, ser. Springer Tracts in Advanced Robotics, 2016, vol. 116.

[18] J. Englsberger, A. Werner, C. Ott, B. Henze, M. A. Roa, G. Garofalo, R. Burger, A. Beyer, O. Eiberger, K. Schmid, and A. Albu-Schäffer, "Overview of the torque-controlled humanoid robot TORO," in *IEEE-RAS Int. Conf. on Humanoid Robots*, 2014, pp. 916 – 923.

[19] B. Henze, A. Werner, M. A. Roa, G. Garofalo, J. Englsberger, and C. Ott, "Control applications of TORO - a torque controlled humanoid robot," in *IEEE-RAS Int. Conf. on Humanoid Robots*, 2014, pp. 841 – 841.

[20] A. Albu-Schäffer, S. Haddadin, C. Ott, A. Stemmer, T. Wimboeck, and G. Hirzinger, "The DLR lightweight robot - design and control concepts in human environments," *Industrial Robot: An Int. Journal*, vol. 34, no. 5, pp. 376 – 385, 2007.

[21] H. J. Ferreau, H. G. Bock, and M. Diehl, "An online active set strategy to overcome the limitations of explicit MPC," *Int. J. of Robust and Nonlinear Control*, vol. 18, no. 8, pp. 816 – 830, 2008.